

## Article

# Experimental Study of Discharging Magnesium-Dissolved Oxygen Seawater Batteries with Various Binder Ratios

 Yimeng Cao, Wanxing Li, Fangzhou Wang , Xiaowen Hao and Jianyu Tan \*

School of New Energy, Harbin Institute of Technology at Weihai, 2, Wenhua Road, Weihai 264209, China

\* Correspondence: wangfz@hit.edu.cn (F.W.); tanjianyu@hitwh.edu.cn (J.T.)

**Abstract:** Magnesium-dissolved oxygen seawater batteries have open structures and flow seawater as electrolytes. These two features attract much attention. The cathode electrode is one of the key components that affect the performance of seawater batteries. In this study, seawater batteries with carbon cathodes made from three commercial carbons were investigated and discussed. The porous structure of the cathode was adjusted by changing the mass ratio between polytetrafluoroethylene (PTFE) and carbon materials. The binder ratios range from 10% to 50%. The structure of the different porous carbon cathodes was characterized, and the discharging performance was analyzed. Results showed that the number of pores with diameters of 2–10 nm decreased as the PTFE ratio increased. Meanwhile, as the PTFE ratio increased from 10% to 50%, the seawater battery discharging voltage and capacity were first inhibited when the PTFE ratio was less than 20% but then promoted. It revealed that a balance should be achieved between the number of reaction sites and the paths for oxygen transfer. Moreover, the oxygen transfer in the porous electrode is more important for batteries working in seawater. This study practically investigates seawater batteries with various PTFE binder ratios and provides a reference for the design of magnesium-dissolved oxygen seawater batteries.

**Keywords:** binder ratio; porous structure; mass transfer; seawater battery



**Citation:** Cao, Y.; Li, W.; Wang, F.; Hao, X.; Tan, J. Experimental Study of Discharging Magnesium-Dissolved Oxygen Seawater Batteries with Various Binder Ratios. *Appl. Sci.* **2023**, *13*, 12996. <https://doi.org/10.3390/app132412996>

Academic Editor: Aliaksandr Shaula

Received: 15 November 2023

Revised: 4 December 2023

Accepted: 4 December 2023

Published: 5 December 2023



**Copyright:** © 2023 by the authors. Licensee MDPI, Basel, Switzerland. This article is an open access article distributed under the terms and conditions of the Creative Commons Attribution (CC BY) license (<https://creativecommons.org/licenses/by/4.0/>).

## 1. Introduction

In recent years, the energy shortage has become a serious problem due to the depletion of fossil fuels [1]. The use of renewable energy is one effective way to address the energy shortage [2]. The development and utilization of renewable energy sources such as wind and solar power require efficient energy storage techniques. Battery energy storage systems are a crucial part of the new power system architecture of the future, allowing the power system to remain resilient and stable under a variety of control methods [3,4]. Many new challenges continue to emerge regarding battery chemistry [5]. Metal-air batteries have gained increasing attention due to their high energy density [6–8]. Metal-air batteries mainly include magnesium-air batteries, lithium-air batteries, sodium-air batteries, and aluminum-air batteries [9,10]. Among them, magnesium-air and lithium-air batteries have theoretical energy densities of up to 6800 Wh/kg [11] and 11,400 Wh/kg [12], respectively.

Magnesium-air batteries use magnesium alloys as anode materials and rely on the reduction reaction of oxygen at the gas diffusion electrode to provide a cathodic current. The battery reaction principles are as follows:



In the research of magnesium-air batteries, there is a type called the magnesium-dissolved oxygen seawater battery [13,14]. This type of battery can directly use seawater as the electrolyte, and therefore, it has several advantages: (i) the battery has a simple and open structure; (ii) the flowing seawater as the electrolyte can alleviate electrode polarization,

improve electrode efficiency and battery stability; (iii) the absence of traditional electrolyte reduces the weight of seawater batteries and avoids a series of safety issues caused by carrying liquid electrolytes.

Previous research found that the mass transfer in the cathode largely affected the battery performance [15–20]. For magnesium-dissolved oxygen seawater batteries, the source of oxygen in the cathode reaction is different from that of conventional metal-air batteries. In conventional metal-air batteries, the required oxygen comes from the air, while in seawater batteries, the majority of the required oxygen comes from dissolved oxygen in seawater. Therefore, the oxygen mass transfer on the cathode significantly affects the performance of seawater batteries. This explains why the cathodes of seawater batteries generally adopt a porous structure to obtain as much oxygen as possible. Moreover, the cathode porous structure affects oxygen mass transfer and further affects the battery's performance. Therefore, researchers have studied the influence of porous cathodes on the performance of metal-air batteries through experiments and simulations. Those studies mainly focus on parameters such as pore size [21–25], surface area [26–29], pore volume [30–33], and cathode wettability [34–37]. Usually, the porous structure of the electrode is determined by the carbon materials and the binder utilized in the electrode.

N Ding et al. [24] conducted research on carbon electrode materials in lithium-oxygen batteries and found that the discharge capacity of the battery was not directly related to the surface area and pore volume of the carbon material. Instead, the discharge capacity is proportional to the pore size within a certain range. To verify this conclusion, the authors used phenolic resin as the carbon precursor and prepared mesoporous and macroporous carbon materials with pore sizes ranging from 20 to 100 nm using silica gel particles with different particle sizes as templates. The results showed that the discharge capacity of the electrodes made from these self-made porous carbons increased with increasing pore size within the range of 20–80 nm, reaching the maximum discharge capacity at a pore size of 80 nm. When the pore size further increased to 100 nm, the discharge capacity gradually decreased. J. Read [25] changed the porous structure of the cathode by altering the formula of the air cathode in lithium-air batteries. Through testing, it was concluded that the discharge capacity increased linearly with the average pore size, while it had no significant relationship with the cathode-specific surface area. Additionally, K. Sakai et al. [26] studied porous cathodes in lithium-air batteries and found that the BET-specific surface area of the cathode does not strongly affect the discharge capacity of the battery. The reason is that the BET-specific surface area mainly depends on the number of micropores with diameters smaller than 2 nm. During the discharge process, the discharge products are prone to block the micropores, preventing oxygen from entering the micropores for the reaction. Therefore, the influence of micropores on oxygen transport in the cathode is negligible. T. Kuboki [30] demonstrated that the discharge capacity of the cathode carbon material is related to the mesopore volume. Furthermore, there has been research on the wettability of cathodes. For example, Wang and Li [34] studied the impact of electrode wettability on the discharge capacity of lithium-air batteries and concluded that hydrophobic electrodes have a higher discharge capacity due to enhanced oxygen diffusion compared to hydrophilic electrodes. Additionally, electrodes with mixed wettability have a higher discharge capacity due to a balanced number of reaction sites and diffusion paths in the electrode. In addition to experiments, simulations have also played a significant role in the study of cathode porous structures. X Li [38] developed a statistical model to study the microstructural evolution of porous electrodes and combined it with computational fluid dynamics models to simulate the discharge performance of the electrode. The results indicated that when the pore size is smaller than the critical pore size, i.e., when the pore is too small to accommodate reactants, pores smaller than the critical size do not have an impact on the discharge capacity of the battery.

Currently, research on metal-air batteries has rarely focused on magnesium-dissolved oxygen seawater batteries. This study primarily investigates the influence of PTFE binder ratios on cathode porous structure and further the performance of magnesium-dissolved

oxygen seawater batteries. In this experiment, carbon electrodes were prepared from three different commercial carbon blacks (acetylene black, VulcanXC-72R, and Ketjen black). The porous structure of the cathode was adjusted by changing the mass ratio of PTFE to the three carbons. Nitrogen adsorption-desorption experiments were performed to characterize the structure of the different porous carbon cathodes. Based on the prepared cathode porous structures, a magnesium-dissolved oxygen seawater battery was designed and fabricated with AZ31 magnesium alloy as the anode material. Constant current discharge tests were conducted to explore the influence of the cathode porous structure on the performance of the magnesium-dissolved oxygen seawater battery.

## 2. Experimental Methods

### 2.1. Electrode Preparation

All purchased commercial materials in this study were used as received. Three types of commercially available carbon blacks (acetylene black, Vulcan XC-72R, and Ketjenblack ECP) were obtained from Xiamen Top New Energy Technology Company (Xiamen, China). Each type of carbon was mixed with polytetrafluoroethylene (PTFE) in different ratios (10%, 20%, 30%, 40%, and 50% by weight of PTFE for each carbon) in isopropanol solution. The corresponding carbon slurries were ultrasonically oscillated for 1 h to ensure thorough mixing of carbon and binder. The slurries were then filtered through a 20-mesh sieve to remove larger particles that could adversely affect the electrode preparation process. The prepared carbon slurries were uniformly coated onto W0S1011 carbon cloth using an LTD model automatic coating machine bought from Xiamen Top New Energy Technology Company (Xiamen, China). The total coating thickness was 300  $\mu\text{m}$ . It was divided into two layers of 150  $\mu\text{m}$  each to prevent cracking after electrode drying. After each coating, the electrodes were dried in ambient air for 6 h, followed by a heat treatment at 350  $^{\circ}\text{C}$  for 30 min to complete the electrode fabrication. The carbon content of different carbon electrodes is shown in Table 1.

**Table 1.** Average carbon mass loadings of different carbon electrodes.

Carbon Electrode	Average Carbon Content (mg/cm <sup>2</sup> )
Acetylene Black	3.19
VulcanXC-72R	3.58
Ketjen Black	3.21

### 2.2. Cell Assembly and Testing

The magnesium-dissolved oxygen seawater battery was designed and assembled according to the schematic diagram in Figure 1. Sea salt solution was used as the electrolyte instead of seawater, and an AZ31B magnesium alloy with dimensions of 3 cm  $\times$  5 cm  $\times$  0.5 cm was used as the anode. The battery structure also included a fixing component and a current collector. The fixing component consisted of four stainless steel hexagon screws and nuts, as well as a white porous resin plate. The current collector consisted of six stainless steel plates. The seawater battery in this experiment employed a dual-cathode structure. Since the cathodic reactant of the seawater battery is not from the air but directly utilizes dissolved oxygen in seawater, a larger cathode area is required to maintain a certain current density. A dual-cathode structure is commonly used to prevent the battery from becoming too large in volume. The porous carbon electrodes were fixed on both sides of the seawater battery, while the magnesium anode was sandwiched between two stainless steel plates. After assembly, the seawater battery was immersed in the electrolyte. The battery testing was conducted using the Neware CT-4000 battery testing system purchase from Neware Technology Limited (Shenzhen, China). The discharge experiments were performed at room temperature with a discharge current intensity of 50 mA. Two cut-off strategies were used: (1) a discharge time of 1 h to obtain the average discharge voltage over 1 h, and (2) a discharge cut-off voltage set at 0.5 V to obtain the specific discharge capacity of the carbon

electrode. The average discharge voltage over 1 h and the specific discharge capacity were used to evaluate the performance of the seawater battery.

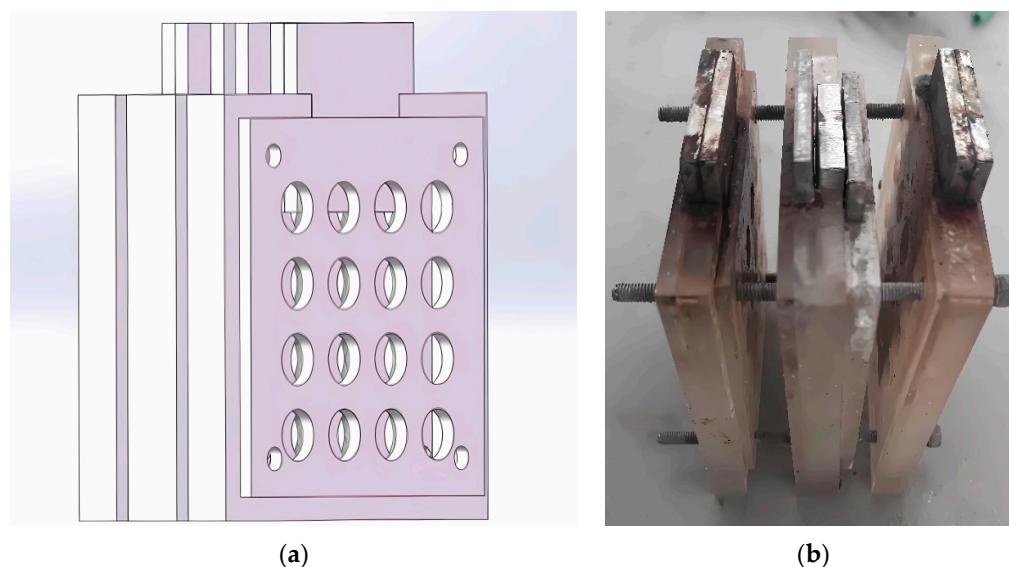


**Figure 1.** (a) Structural diagram of seawater battery; (b) seawater battery prototype.

### 2.3. Nitrogen Adsorption and Desorption

All carbon samples were characterized using a surface area and pore size analyzer (ASAP2460) bought from micromeritics (Shanghai, China). The adsorption and desorption isotherms were obtained by performing physical adsorption measurements at 77 K after pre-treating the carbon samples under vacuum heating at 180 °C for 4 h. After obtaining the isotherms, the BET method was used to analyze the specific surface area, and the BJH method was employed to evaluate pore volume and pore size distribution.

## 3. Results and Discussion

### 3.1. Porous Structure Characterization

The carbon electrodes with a binder weight ratio of 10% are named Acetylene Black-10%, and the naming method for the remaining carbon electrodes follows the same pattern. The structural characterization of the carbon electrodes with different binder ratios is summarized in Figures 2 and 3. The nitrogen adsorption and desorption isotherms are provided in the supplementary file. Type IV isotherms are clearly observed for the Acetylene Black, Vulcan XC-72R, and Ketjen Black carbon electrodes, indicating the presence of mesoporous structures in carbon electrodes. In Figure 2, low binder ratio carbon electrodes show a more specific surface area. This is because more micropores are detected. High binder ratio carbon electrodes hardly exhibit any micropores. This is due to the significant reduction in the number of micropores in carbon electrodes with increased binder content, as confirmed by previous studies [15]. The average pore size for each carbon electrode is presented in Figure 3. As the binder ratio increases, the average pore size of the carbon electrode increases continuously. The addition of binders has a minor influence on mesopores and macropores but has an obvious effect on the micropores. Adding more binders can block more micropores, which will not be filled by nitrogen in the gas sorption experiment. The reduction in micropore volume results in an increased proportion of mesopores and macropores, leading to an increase in the average pore size of the carbon electrode with an increasing binder ratio. This is further confirmed by the pore size distribution of carbon electrodes with different binder ratios shown in Figure 4. Figure 4a illustrates that for the Acetylene Black carbon electrode, the proportion of pores in the 30–50 nm range increases with increasing binder ratio in the range of 10–50%, resulting in a larger average pore size. In addition, the change in the average pore size is also affected by the preparation process

and the testing method, resulting in some differences in the trend of Figure 3. Additionally, Figure 4b,c shows that as the binder ratio gradually increases within the range of 10–50%, the slope of the pore size distribution curve in the 2–10 nm range decreases for the Vulcan XC-72R and Ketjen Black carbon electrodes. This presents a decreasing proportion of pores in the 2–10 nm range. Figure 4b,c provides an increased proportion of pores in the 10–50 nm range for Vulcan XC-72R and Ketjen Black carbon electrodes, thus improving the utilization of mesopores and macropores in the carbon electrode and facilitating oxygen diffusion. Furthermore, the addition of binders affects the wettability of the carbon electrode. As PTFE is hydrophobic, the wettability of the electrode decreases with an increasing binder ratio, resulting in a reduced number of reaction sites on the carbon electrode. However, the decrease in wettability also promotes the diffusion of oxygen in non-wetting pores, as previously demonstrated in Ref. [34].

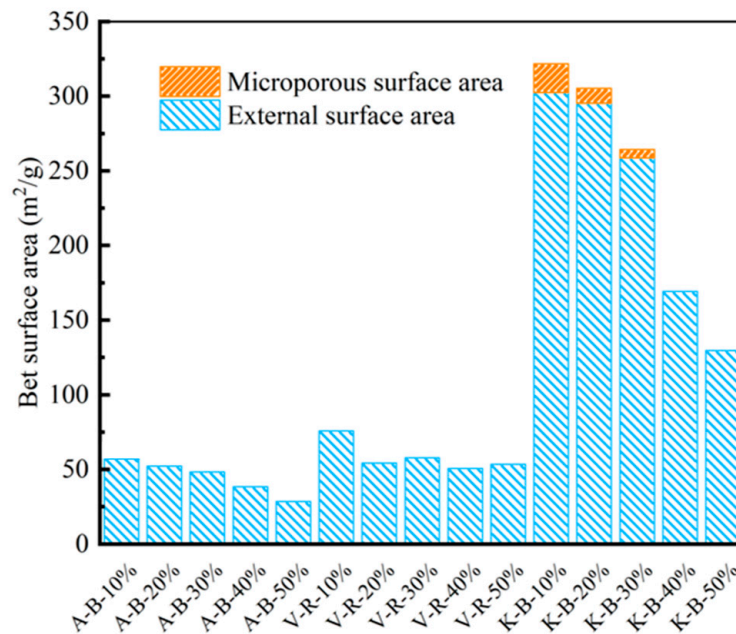


Figure 2. Specific surface areas of different carbon electrodes.

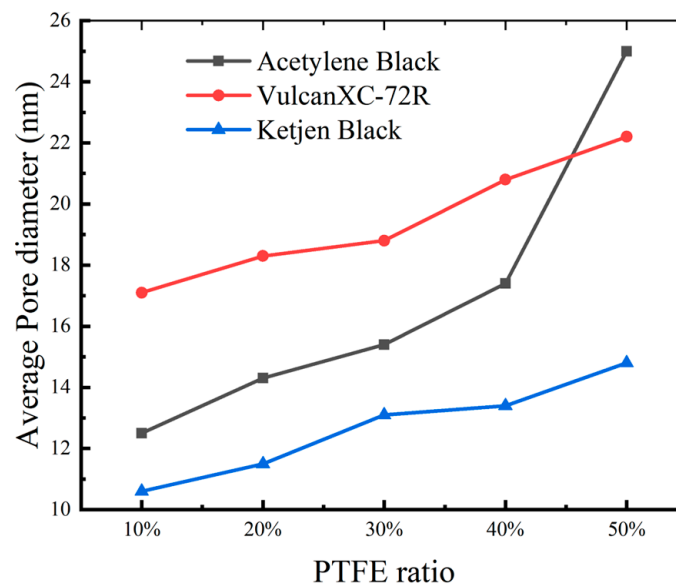
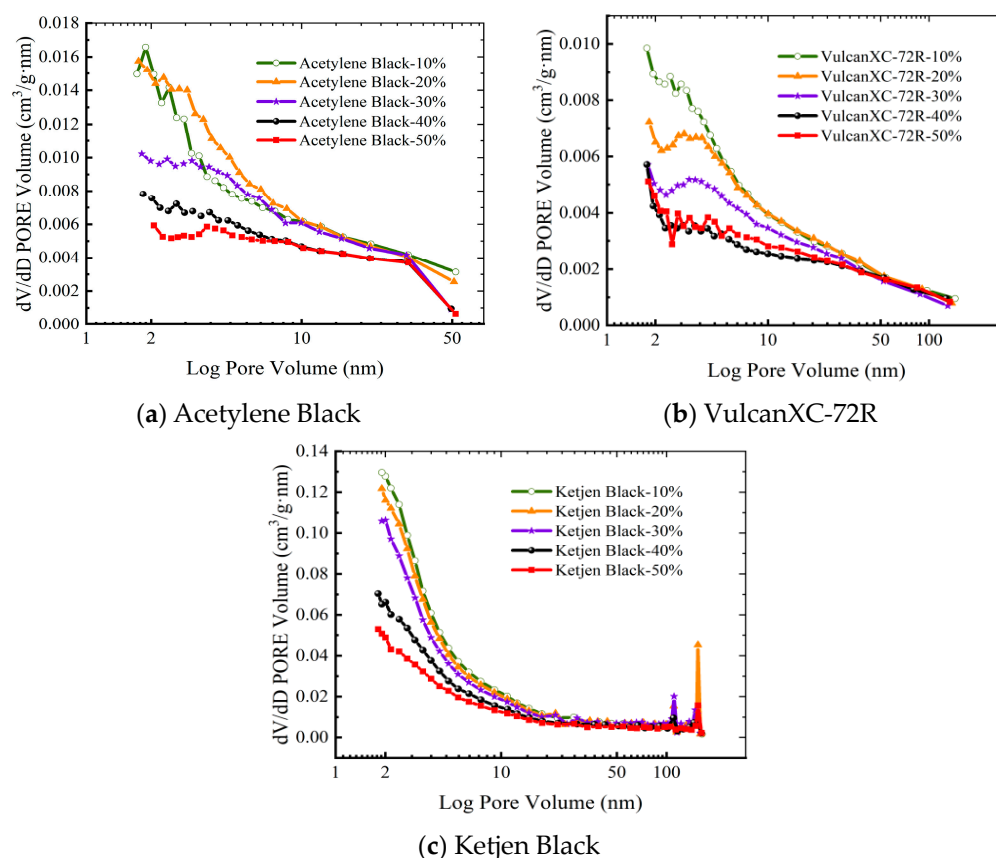


Figure 3. The average pore diameter of different carbon electrodes.



**Figure 4.** Pore size distribution of different carbon electrodes.

### 3.2. Discharge Performance

Based on the aforementioned different carbon electrodes, magnesium dissolution oxygen seawater cells were assembled with an AZ31 magnesium alloy as the anode. These cells were subjected to a constant current discharge of 50 mA for one hour to obtain the average discharge voltage for each carbon electrode (with at least three discharge experiments conducted for each carbon electrode). As shown in Figure 5, for the same carbon electrode with different binder ratios, the average discharge voltage for one hour initially decreases and then increases as the binder ratio increases within the range of 20–50%. The minimum value is observed at a binder ratio of 20%, while the maximum is reached at a binder ratio of 50%. The reason for this phenomenon is that the binder PTFE affects the porous structure and wettability of the carbon electrode, which in turn affects the oxygen diffusion process on the electrode. Increasing the binder ratio from 10% to 20%, the wettability of the carbon electrode decreases, the number of electrochemical reaction sites decreases, and the discharge reaction is limited to a certain extent, which leads to a decrease in the average discharge voltage at a binder ratio of 20%. However, the binder ratio was further increased to 50%, and the lower wettability increased the diffusion of oxygen in the non-wetted pores, which in turn enhanced the overall diffusion of oxygen within the porous structure. At the same time, the addition of PTFE increases the percentage of pores with larger pore sizes in the carbon electrode, increasing the utilization of larger-sized pores in the carbon electrode, and the high utilization of mesoporous and above pores is also conducive to the enhancement of oxygen diffusion. Therefore, the average discharge voltage increases when the binder ratio increases from 20% to 50%. In Figure 5, it is observed that the voltage generally increases and then decreases in discharge curves. This is because the anode magnesium alloy samples have an oxide film attached to the outside, which is first consumed to activate the electrode when the discharge reaction takes place. It is a common phenomenon during the repetition of experiments. Figure 5 also indicates

that for carbon electrodes with the same binder ratio, the Ketjen Black carbon electrode exhibits the highest average discharge voltage for one hour, followed by the Acetylene Black carbon electrode. The Vulcan XC-72R carbon electrode shows the lowest value. For example, at a binder ratio of 30%, the average voltage for one hour is 1.08 V for Acetylene Black-30% carbon electrode, 1.02 V for Vulcan XC-72R-30% carbon electrode, and 1.13 V for Ketjen Black-30% carbon electrode. As shown in Figure 2, the Ketjen Black carbon electrode has the largest specific surface area, and the number of its reaction sites is higher than the other two electrodes at low binder ratios. In Figure 4, the Ketjen Black carbon electrode has a higher macroporous capacity than both other electrodes. This indicates it has a better oxygen transport capacity at higher binder ratios, resulting in a higher discharge capacity.

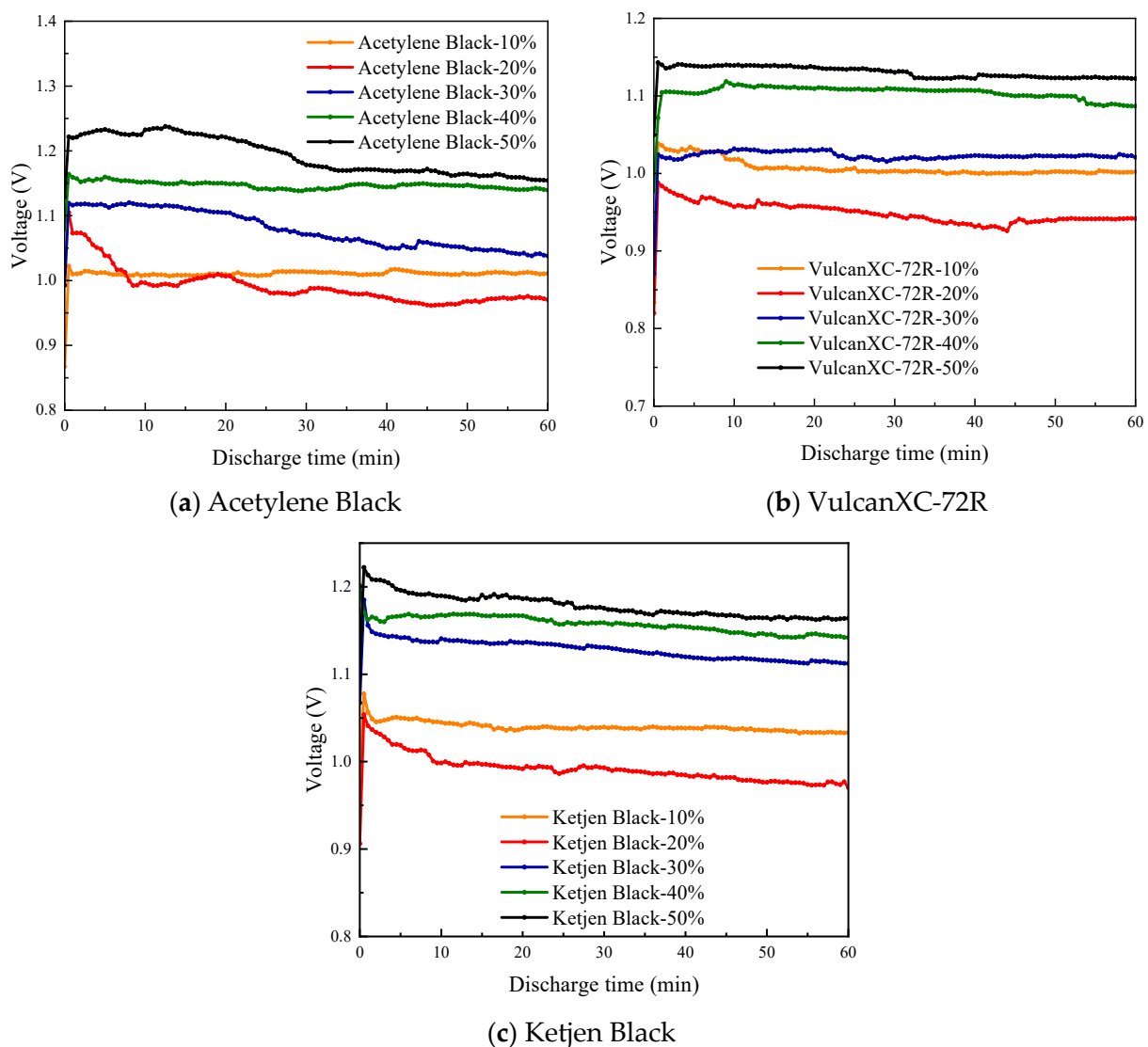


**Figure 5.** One-hour average discharge voltage of different carbon electrodes.

As a result, the Ketjen Black carbon electrode has the highest average discharge voltage among the three carbon electrodes, especially when the binder percentage is greater than 30%. For the Ketjen Black carbon electrode, when the proportion of binder is greater than 30%, the proportion of “large holes” in the carbon electrode is significantly more than the rest of the carbon electrodes, so the average discharge voltage is significantly better than the rest of the carbon electrodes.

All carbon electrodes underwent single deep discharge specific capacity testing at a current intensity of 50 mA. Due to the low specific surface area, the discharge capacity

of the original carbon cloth was neglected, and the discharge specific capacity in this experiment was calculated only based on the weight of the commercial carbons coated on the electrodes, excluding the weight of the original carbon cloth substrate and binders. Each carbon electrode was tested three times, and the average of the three test results was taken as the experimental result. The single deep discharge capacity comparison is shown in Figure 6. When the binder ratio is within the range of 10–50%, the single deep discharge specific capacity of the three different carbon electrodes initially decreases and then increases. The minimum value is observed at a binder ratio of 20%, while the maximum is reached at a binder ratio of 50%. Among them, the Ketjen Black carbon electrode with a 50% PTFE coating achieved the highest discharge specific capacity of 11.86 Ah/g.

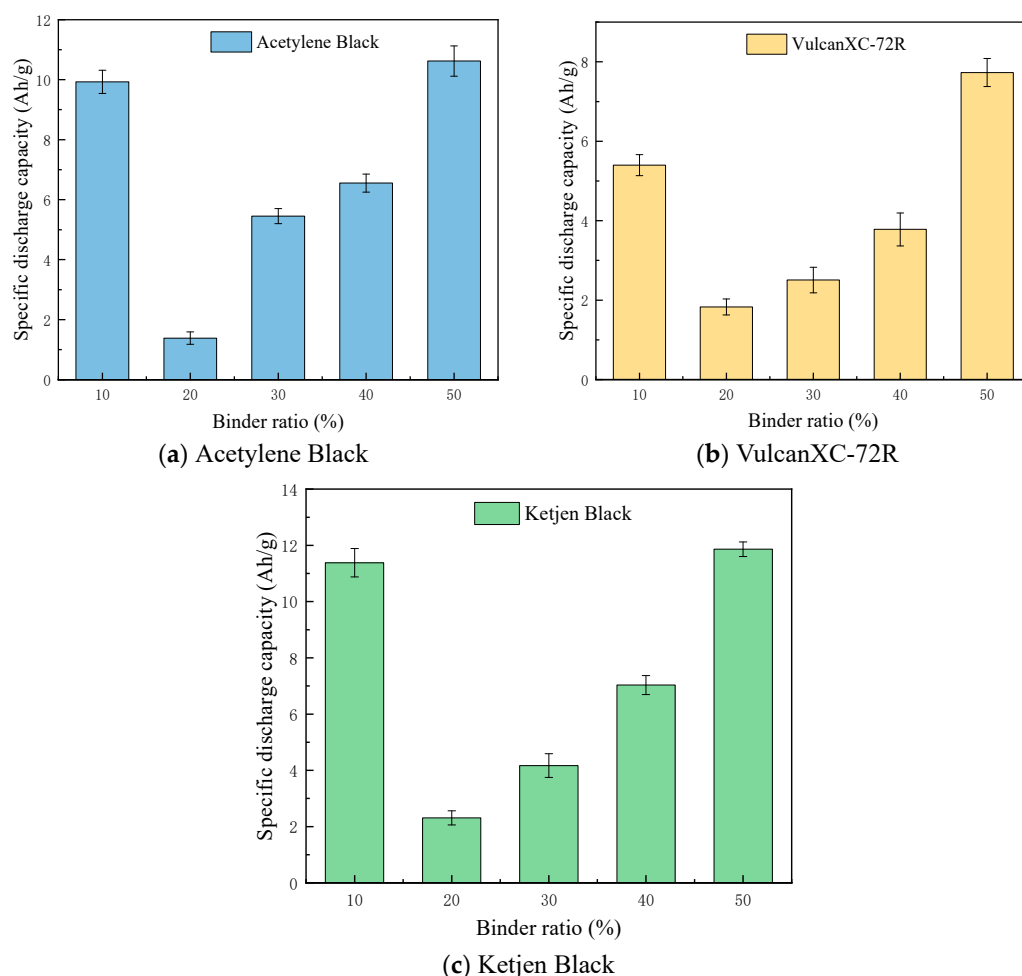


**Figure 6.** Depth discharge of the different carbon electrodes.

The average discharge voltage for one hour and the single deep discharge specific capacity are adopted as indicators of the seawater battery performance. Combined with the results of the one-hour constant current discharge experiment, it is evident that when the binder ratio is within the range of 10–50%, the performance of the carbon electrode initially decreases and then promotes with the increase in the binder ratio. The performance is the worst at a binder ratio of 20% and the best at a binder ratio of 50%. The detailed analyses are shown as follows.

Before the detailed discussion on those results, it should be clarified that the battery usually works in seawater. Thus, the oxygen supply for the electrochemical reaction is mainly affected by the oxygen dissolved in the seawater and oxygen transfer in the porous electrode. Based on the experimental results shown in Figures 5 and 6, when the binder ratio is less than 20%, the performance of the three carbon electrodes worsens with the

increase in the binder ratio. Seawater batteries use seawater as the electrolyte, and the dissolved oxygen in seawater is low. When the binder ratio is less than 20%, most of the electrode surface is wetted and the dissolved oxygen meets the demand of the reaction. The wetted surface (active reaction sites) dominates the battery performance. Therefore, when the proportion of binder increases from 10% to 20%, the electrode wettability decreases, leading to a decrease in battery performance. When the binder ratio is greater than 20%, the performance of the three carbon electrodes becomes better with the increase in the binder ratio. Although the number of reaction sites decreases within these binder ratios, the higher binder ratio has a greater impact on the wettability and porous structure of the carbon electrode. The decrease in electrode wettability enhances oxygen diffusion in non-wetted pores, and the increase in the binder ratio increases the proportion of mesopores and macropores in the carbon electrode, improving the utilization of mesopores and macropores. Both promote oxygen transfer, improving oxygen supply and enhancing cell performance. At this point, oxygen transfer has the primary influence on the cell performance. This is the reason for the initial decrease and subsequent increase in the performance of the seawater cell with increasing binder ratio.

In summary, under the same test conditions and the same PTFE ratio, the average discharge voltage follows the order of Ketjen Black > Acetylene Black > VulcanXC-72R. The single deep discharge specific capacity follows the order of Ketjen Black > Acetylene Black > VulcanXC-72R. Therefore, it can be concluded that the Ketjen Black carbon electrode exhibits the best performance in this study. Moreover, after adding the binder, the utilization of mesopores and macropores in the Ketjen Black carbon electrode is higher than that in Acetylene Black and VulcanXC-72R carbon electrodes. Further, when the binder ratio is higher than 50%, the performance of the battery may be reduced. Excessive binder content will result in a significant reduction in electrode conductivity. Low electric conductivity then has a negative effect on discharging the battery [39]. In addition, the over-binder-covered electrode surface makes the electrode surface less homogeneous, resulting in electrode instability possibly shortening its life [40]. Therefore, the content of PTFE has to be strictly controlled to ensure that the optimum performance is obtained within the battery.

#### 4. Conclusions

We prepared three kinds of porous carbon electrodes with different PTFE ratios for magnesium-dissolved oxygen seawater cells. Structural characterization of all carbon electrodes was conducted using nitrogen adsorption-desorption experiments. Based on the prepared carbon electrodes, magnesium-dissolved oxygen seawater cells were assembled and subjected to constant current discharge testing, leading to the following conclusions:

(1) When the PTFE ratio in the carbon electrode is within the range of 10–50%, the number of micropores and pores with diameters in the range of 2–10 nm decreases continuously, while the average pore size of the carbon electrode increases. The specific surface area of the carbon electrode is mainly affected by micropores and small-sized pores, which decreases as the PTFE ratio increases.

As the binder ratio increases, the average pore size of the carbon electrode increases continuously.

(2) When the PTFE ratio is within the range of 10–50%, the performance of the magnesium-dissolved oxygen seawater cell initially decreases and then increases. In the working environment where oxygen is hard to acquire, when the PTFE ratio in the carbon electrode is less than 20%, it is speculated the performance of the seawater cell is mainly influenced by the number of reaction sites. An increase in the PTFE ratio leads to a decrease in the performance of the seawater cell. When the PTFE ratio in the carbon electrode is greater than 20%, the performance of the seawater cell is primarily influenced by oxygen diffusion on the carbon electrode. An increase in the PTFE ratio enhances the performance of the seawater cell.

(3) Among the different carbon electrodes with the same PTFE ratio, the Ketjen Black carbon electrode exhibits the best performance. The single deep discharge specific capacity of the Ketjen Black carbon electrode with a 50% PTFE ratio can reach 11.86 Ah/g, followed by the Acetylene Black carbon electrode, and the VulcanXC-72R carbon electrode performs the worst. The electrode with a binder ratio over 50% is not recommended since it can significantly reduce the electrical conductivity.

**Supplementary Materials:** The following supporting information can be downloaded at: <https://www.mdpi.com/article/10.3390/app132412996/s1>. Figure S1: N<sub>2</sub> adsorption-desorption isotherms of different carbon electrodes.

**Author Contributions:** Conceptualization, F.W.; methodology, X.H.; formal analysis, W.L.; investigation, Y.C.; resources, F.W.; data curation, X.H.; writing—original draft preparation, Y.C.; writing—review and editing, W.L.; funding acquisition, F.W. and J.T. All authors have read and agreed to the published version of the manuscript.

**Funding:** This research was funded by the National Natural Science Foundation of China (Grant No. 52006046) and the Key R&D Program of Shandong Province, China (2022ZLGX04).

**Institutional Review Board Statement:** Not applicable.

**Informed Consent Statement:** Not applicable.

**Data Availability Statement:** The data can be available for research purposes only. All those interested can contact the author directly via email. The data are not publicly available due to privacy.

**Conflicts of Interest:** The authors declare no conflict of interest.

## References

1. Yao, T.L.; Huang, J.L.; Li, Z.W.; Liu, Q.; Li, J.; Jiang, K.; Yan, X.; Liu, N. Planning Scheme Design for Multi-time Scale Energy Storage at the City Level. In Proceedings of the 58th IEEE/IAS Industrial and Commercial Power Systems Technical Conference Asia (IEEE I and CPS Asia), Shanghai, China, 8–11 July 2022.
2. Wang, F.; Kahol, P.K.; Gupta, R.; Li, X. Experimental Studies of Carbon Electrodes With Various Surface Area for Li–O<sub>2</sub> Batteries. *J. Electrochem. Energy Convers. Storage* **2019**, *16*, 041007. [[CrossRef](#)]
3. Lung, L.-Y.; Chou, T.-Y.; Chang, W.-C.; Kuo, C.-C. Development of Energy Storage Systems for High Penetration of Renewable Energy Grids. *Appl. Sci.* **2023**, *13*, 11978. [[CrossRef](#)]
4. Saravanakumar, Y.N.; Sultan, M.T.H.; Shahar, F.S.; Giernacki, W.; Łukaszewicz, A.; Nowakowski, M.; Holovatyy, A.; Stepień, S. Power Sources for Unmanned Aerial Vehicles: A State-of-the Art. *Appl. Sci.* **2023**, *13*, 11932. [[CrossRef](#)]
5. Vegge, T.; Garcia-Lastra, J.M.; Siegel, D.J. Lithium-oxygen batteries: At a crossroads? *Curr. Opin. Electrochem.* **2017**, *6*, 100–107. [[CrossRef](#)]
6. Chen, Y.H.; Xu, J.J.; He, P.; Qiao, Y.; Guo, S.; Yang, H.; Zhou, H. Metal-air batteries: Progress and perspective. *Sci. Bull.* **2022**, *67*, 2449–2486. [[CrossRef](#)] [[PubMed](#)]
7. Reddy, V.P.; Blanco, M.; Bugga, R. Boron-based anion receptors in lithium-ion and metal-air batteries. *J. Power Sources* **2014**, *247*, 813–820. [[CrossRef](#)]
8. Zhang, X.; Wang, X.G.; Xie, Z.J.; Zhou, Z. Recent progress in rechargeable alkali metal-air batteries. *Green Energy Environ.* **2016**, *1*, 4–17. [[CrossRef](#)]
9. Wang, F.; Liang, C.S.; Xu, D.L.; Cao, H.-Q.; Sun, H.-Y.; Luo, Z.-K. Research Progress of Lithium-air Battery. *J. Inorg. Mater.* **2012**, *27*, 1233–1242. [[CrossRef](#)]
10. Aurbach, D.; McCloskey, B.D.; Nazar, L.F.; Bruce, P.G. Advances in understanding mechanisms underpinning lithium-air batteries. *Nat. Energy* **2016**, *1*, 16128. [[CrossRef](#)]
11. Yu, Z.; Shi, G.; Ju, D.Y. Electrochemical Properties Evaluation of a Novel Mg Alloy Anode on Mg-1 Air Batteries. *Int. J. Electrochem. Sci.* **2014**, *9*, 6668–6676.
12. Rahman, M.A.; Wang, X.J.; Wen, C.E. High Energy Density Metal-Air Batteries: A Review. *J. Electrochem. Soc.* **2013**, *160*, A1759–A1771. [[CrossRef](#)]
13. Yu, J.X.; Ma, L.; Duan, T.G.; Xin, Y.; Lv, Y.; Zhang, H. Electrocatalytic oxygen reduction of three-dimensional carbon fiber-based composites for seawater oxygen-dissolved battery. *Carbon Lett.* **2022**, *32*, 537–546. [[CrossRef](#)]
14. Wilcock, W.S.D.; Kauffman, P.C. Development of a seawater battery for deep-water applications. *J. Power Sources* **1997**, *66*, 71–75. [[CrossRef](#)]
15. Song, J.; Ji, Y.; Li, Y.; Tong, R.; Tian, Q.; Chen, J.; Chen, Z. Porous carbon with carbon nanotube scaffold for embedding Cu<sub>2</sub>O/Cu nanoparticles towards high lithium storage. *Chem. Phys. Lett.* **2021**, *780*, 138934. [[CrossRef](#)]

16. Wu, A.; Li, C.; Han, B.; Hanson, S.; Guan, W.; Singhal, S.C. Effect of air addition to the air electrode on the stability and efficiency of carbon dioxide electrolysis by solid oxide cells. *Int. J. Hydrogen Energy* **2022**, *47*, 24268–24278. [[CrossRef](#)]
17. Rao, Y.; Zhong, S.; He, F.; Wang, Z.; Peng, R.; Lu, Y. Cobalt-doped BaZrO<sub>3</sub>: A single phase air electrode material for reversible solid oxide cells. *Int. J. Hydrogen Energy* **2012**, *37*, 12522–12527. [[CrossRef](#)]
18. Kuanusont, N.; Shimoyama, Y. Porous carbon electrode for Li-air battery fabricated from solvent expansion during supercritical drying. *J. Supercrit. Fluids* **2018**, *133*, 77–85. [[CrossRef](#)]
19. Ishihara, T.; Yokoe, K.; Miyano, T.; Kusaba, H. Mesoporous MnCo<sub>2</sub>O<sub>4</sub> spinel oxide for a highly active and stable air electrode for Zn-air rechargeable battery. *Electrochim. Acta* **2019**, *300*, 455–460. [[CrossRef](#)]
20. Milikić, J.; Nastasić, A.; Martins, M.; Sequeira, C.A.C.; Šljukić, B. Air Cathodes and Bifunctional Oxygen Electrocatalysts for Aqueous Metal–Air Batteries. *Batteries* **2023**, *9*, 394. [[CrossRef](#)]
21. Williford, R.E.; Zhang, J.-G. Air electrode design for sustained high power operation of Li/air batteries. *J. Power Sources* **2009**, *194*, 1164–1170. [[CrossRef](#)]
22. Lin, C.; Li, X.; Shinde, S.S.; Kim, D.H.; Song, X.; Zhang, H.; Lee, J.H. Long-life rechargeable Zn air battery based on binary metal carbide armored by nitrogen-doped carbon. *ACS Appl. Energy Mater.* **2019**, *2*, 1747–1755. [[CrossRef](#)]
23. Tian, W.-W.; Ren, J.-T.; Lv, X.-W.; Yuan, Z.Y. A “gas-breathing” integrated air diffusion electrode design with improved oxygen utilization efficiency for high-performance Zn-air batteries. *Chem. Eng. J.* **2022**, *431*, 133210. [[CrossRef](#)]
24. Ding, N.; Chien, S.W.; Hor, T.A.; Lum, R.; Zong, Y.; Liu, Z. Influence of carbon pore size on the discharge capacity of Li–O<sub>2</sub> batteries. *J. Mater. Chem. A* **2014**, *2*, 12433–12441. [[CrossRef](#)]
25. Read, J. Characterization of the lithium/oxygen organic electrolyte battery. *J. Electrochem. Soc.* **2002**, *149*, A1190–A1195. [[CrossRef](#)]
26. Sakai, K.; Iwamura, S.; Mukai, S.R. Influence of the Porous Structure of the Cathode on the Discharge Capacity of Lithium-Air Batteries. *J. Electrochem. Soc.* **2017**, *164*, A3075–A3080. [[CrossRef](#)]
27. Ou, Z.H.; Qin, Y.; Xue, C.L.; Lum, R.; Zong, Y.; Liu, Z. Double-activator modulation of ultrahigh surface areas on doped carbon catalysts boosts the primary Zn–Air battery performance. *ACS Appl. Energy Mater.* **2022**, *5*, 1701–1709. [[CrossRef](#)]
28. Hayashi, M.; Minowa, H.; Takahashi, M.; Shodai, T. Surface Properties and Electrochemical Performance of Carbon Materials for Air Electrodes of Lithium-Air Batteries. *Electrochemistry* **2010**, *78*, 325–328. [[CrossRef](#)]
29. Ferreira, J.; Salgueiro, T.; Marcuzzo, J.; Arruda, E.; Ventura, J.; Oliveira, J. Textile PAN Carbon Fibers Cathode for High-Voltage Seawater Batteries. *Batteries* **2023**, *9*, 178. [[CrossRef](#)]
30. Kuboki, T.; Okuyama, T.; Ohsaki, T.; Takami, N. Lithium-air batteries using hydrophobic room temperature ionic liquid electrolyte. *J. Power Sources* **2005**, *146*, 766–769. [[CrossRef](#)]
31. Léonard, A.F.; Castro-Muniz, A.; Suarez-Garcia, F.; Job, N.; Paredes, J.I. Understanding the effect of the mesopore volume of ordered mesoporous carbons on their electrochemical behavior as Li-ion battery anodes. *Microporous Mesoporous Mater.* **2020**, *306*, 110417. [[CrossRef](#)]
32. Peng, H.; Ma, G.F.; Sun, K.J.; Mu, J.; Lei, Z. One-step preparation of ultrathin nitrogen-doped carbon nanosheets with ultrahigh pore volume for high-performance supercapacitors. *J. Mater. Chem. A* **2014**, *2*, 17297–17301. [[CrossRef](#)]
33. Kim, M.J.; Park, J.E.; Kim, S.; Lim, M.S.; Jin, A.; Kim, O.H.; Kim, M.J.; Lee, K.S.; Kim, J.; Kim, S.S.; et al. Biomass-derived air cathode materials: Pore-controlled S, N-Co-doped carbon for fuel cells and metal–air batteries. *ACS Catal.* **2019**, *9*, 3389–3398. [[CrossRef](#)]
34. Wang, F.; Li, X. Effects of the Electrode Wettability on the Deep Discharge Capacity of Li–O<sub>2</sub> Batteries. *ACS Omega* **2018**, *3*, 6006–6012. [[CrossRef](#)] [[PubMed](#)]
35. Zheng, H.; Zhou, X.; Cheng, S.; Xia, R.; Nie, S.; Liang, X.; Sun, Y.; Xiang, H. High-Voltage LiNi<sub>0.5</sub>Mn<sub>1.5</sub>O<sub>4</sub> Cathode Stability of Fluorinated Ether Based on Enhanced Separator Wettability. *J. Electrochem. Soc.* **2019**, *166*, A1456–A1462. [[CrossRef](#)]
36. Schroder, A.; Wippermann, K.; Zehl, G.; Stolten, D. The influence of cathode flow field surface properties on the local and time-dependent performance of direct methanol fuel cells. *Electrochem. Commun.* **2010**, *12*, 1318–1321. [[CrossRef](#)]
37. Li, J.; Ye, D.D.; Zhu, X.; Liao, Q.; Ding, Y.D.; Tian, X. Effect of wettability of anode microporous layer on performance and operation duration of passive air-breathing direct methanol fuel cells. *J. Appl. Electrochem.* **2009**, *39*, 1771–1778. [[CrossRef](#)]
38. Li, X. A Modeling Study of the Pore Size Evolution in Lithium-Oxygen Battery Electrodes. *J. Electrochem. Soc.* **2015**, *162*, A1636–A1645. [[CrossRef](#)]
39. Liu, B.; Dai, Y.K.; Li, L.; Zhang, H.D.; Zhao, L.; Kong, F.R.; Sui, X.L.; Wang, Z.B. Effect of polytetrafluoroethylene (PTFE) in current collecting layer on the performance of zinc-air battery. *Prog. Nat. Sci. Mater. Int.* **2020**, *30*, 861–867. [[CrossRef](#)]
40. Liu, S.; Wippermann, K.; Lehnert, W. Mechanism of action of polytetrafluoroethylene binder on the performance and durability of high-temperature polymer electrolyte fuel cells. *Int. J. Hydrogen Energy* **2021**, *46*, 14687–14698. [[CrossRef](#)]

**Disclaimer/Publisher’s Note:** The statements, opinions and data contained in all publications are solely those of the individual author(s) and contributor(s) and not of MDPI and/or the editor(s). MDPI and/or the editor(s) disclaim responsibility for any injury to people or property resulting from any ideas, methods, instructions or products referred to in the content.